UNIVERSITAT POLITÈCNICA
DE CATALUNYA
BARCELONATECH

UPCommons

Portal del coneixement obert de la UPC

http://upcommons.upc.edu/e-prints

This is the peer reviewed version of the following article: Liu, Q. [et al.]. Inverse Optical Cavity Design for Ultrabroadband Light Absorption Beyond the Conventional Limit in Low-Bandgap Nonfullerene Acceptor–Based Solar Cells. *Advanced energy materials*, 23 Maig 2019, vol. 9, núm. 20, p. 1-8, which has been published in final form at DOI: <10.1002/aenm.201900463>.

This article may be used for non-commercial purposes in accordance with Wiley Terms and Conditions for Use of Self-Archived Versions.

DOI: 10.1002/ ((please add manuscript number))

Article type: (Full Paper**)**

Title: Inverse optical cavity design for ultrabroadband light absorption beyond the conventional limit in low-bandgap nonfullerene acceptor based solar cells

Quan Liu,[1] Johann Toudert,[1] Tengfei Li,[2] Mariia Kramarenko,[1] Guillermo Martínez-Denegri,[1] Laura Ciammaruchi,[1] Xiaowei Zhan[2] and Jordi Martorell[1,3*]*

[1]ICFO-Institut de Ciencies Fotoniques, The Barcelona Institute of Science and Technology, 08860 Castelldefels (Barcelona), Spain

[2]Department of Materials Science and Engineering, College of Engineering

Key Laboratory of Polymer Chemistry and Physics of Ministry of Education, Peking University, Beijing 100871, China

[3]Departament de Física, Universitat Politècnica de Catalunya, 08222 Terrassa, Spain

[*]Corresponding authors E-mail: xwzhan@pku.edu.cn, jordi.martorell@icfo.es

Keywords: Light trapping, optical cavity, ternary blend, low-bandgap nonfullerene acceptor thin-film solar cell

Abstract

In the sub-wavelength regime several nanophotonic configurations have been proposed to overcome the conventional light trapping or light absorption enhancement limit in solar cells also known as the Yablonovitch limit. It was recently suggested that establishing such limit should rely on computational inverse electromagnetic design instead of the traditional approach combining intuition and a priori known physical effect. In here, by applying an inverse full wave vector electromagnetic computational approach, we designed a 1-dimensionl nano-structured optical cavity with a new resonance configuration that provides an ultra-broadband (~ 450 nm) light absorption enhancement when applied to a 107 nm thick active layer organic solar cell based on a low-bandgap (1.32 eV) nonfullerene acceptor. We demonstrate computationally and experimentally that the absorption enhancement provided by such cavity surpasses the conventional limit resulting from an ergodic optical geometry by a 7 % average over a 450 nm band and by more than 20% in the NIR. In such cavity configuration the solar cells exhibited a maximum power conversion efficiency above 14%, corresponding to the highest ever measured for devices based on the specific nonfullerene acceptor we used.

1. Introduction

In any kind of solar cell, when light absorption is weak as a consequence of a small absorption coefficient α and/or a small thickness ℓ for the active layer, light trapping becomes the only possible route to achieve an optimal device performance. By roughening the light entering cell surface with the aim to obtain an ergodic optical geometry, one may reach what is known as the Yablonovitch or conventional limit for light trapping.[1] In such limit, the maximum enhancement for photon absorption can be determined to be $4n^2$ from the fraction of absorbed light energy (f_{abs}) given, when $\alpha\ell \ll 1$, by

$$f_{abs} = \frac{\alpha\ell}{\alpha\ell + \frac{1}{4n^2}} \quad (1)$$

where n is the refractive index of the active layer [2–4]. When the cell architecture is composed of several layers with a thickness, including that of the active layer, smaller than the wavelength, the available modes for light propagation may change significantly and the continuum density of states used to derive the conventional light trapping limit is no longer applicable. It has been shown that in such sub-wavelength regime and for a limited wavelength range, one may overcome the conventional limit following different approaches to trap light.[5–12] In the majority of such cases, to establish the limit for light absorption enhancement, the approach relied in an intuition based nano-structure design supported by a rigorous electromagnetic field distribution computation. However, it was recently suggested that the optimal sub-wavelength structure to reach the light trapping limit should be sought by using computational inverse electromagnetic design.[13] It was demonstrated that for the frequency range ($\lesssim 100\ nm$) with the largest number of sun photons and in the limit of very weak absorption ($\alpha\ell \ll 1$), interface 3-dimensional nano-structures could be designed to obtain cell configurations that would perform roughly 30% better than randomly textured ones.[10] Unfortunately, the final configuration proposed would not be applicable to many thin

film cells exhibiting light absorption deficiency, such as for instance in organic material based cells, provided the absorption band in such cells is several hundreds of nanometers wide and $\alpha\ell \sim 1$.

Here, we use an inverse electromagnetic computational approach to design a 1-dimensional nano-structured optical cavity with an ultra-broadband (~ 450 nm) light trapping capacity, which we use to enhance light absorption in a 107 nm thick active layer organic solar cell. We demonstrate, computationally and experimentally, that for a 450 nm band the absorption enhancement obtained by such novel optical cavity design approach surpasses by an average of 7% the conventional limit based on an ergodic optical geometry. In the NIR, configurations for the cavity are found such that the conventional limit is surpassed by even more than 20%. The organic cells we fabricated are based on the fused tris(thienothiophene) derivative FOIC nonfullerene acceptor (NFA) [14] that exhibits a bandgap which is very close to the ideal 1.34 eV predicted by the Shockley-Queisser theory.[15] We used non-fullerene acceptors provided they exhibit a relatively smaller voltage loss[16–23] and a better absorption tunability[24–32] when compared to their fullerene counterparts. We demonstrated that the light trapping provided by the cavity leads to cells exhibiting power conversion efficiencies (PCEs) above 14%, the highest ever measured when using such type of NFA.

2. Results and discussion

2.1 Optical cavity inverse design

As it has been noted in several occasions light trapping in thin film cells may be enhanced by replacing the standard ITO transparent electrode by an ultra-thin Ag layer.[33–37] Although the 1-dimensional layered architecture between the substrate/cell interface and the back metal electrode is quite simple, it forms an optical cavity with a rather complex resonance structure. Such optical cavity is composed of an absorber layer sandwiched between a 100 nm thick

back Ag layer and a dielectric/metal layer (DML) structure, being the thickness of the metal, typically Ag, around 10 nm or more. To better understand light trapping in such cavity structure, shown in Figure 1a, we consider the electromagnetic energy storing capacity in two limiting cases. When the front Ag layer is made as thick as a few tens of nm, resonances are found, as seen in the Figure S1 (Supporting Information), for $m\lambda/2 = L$, where m is a positive integer and L may be assumed to be close to the total cavity length. In the opposite limit, when the thickness of the front Ag is equal to zero, the resonance structure, shown in Figure 1b, is very different and does not seem to relate in any obvious way to the total cavity length. To experimentally confirm both energy storage resonance structures, we fabricated both types of cavities replacing the absorber layer by a non-absorbing MoO_3 layer which has a refractive index close to the index of the organic blend that we use in the cells we fabricate. The energy storing capacity can be estimated through the transmission spectrum when thinning down the back Ag layer from 100 nm down to 25 nm. The light transmission measurements confirm that the resonances from the two limiting cavities are degenerate only for some very specific cavity configurations, as seen in Figure 1c. When comparing Figure 1b and 1c note that reducing the thickness of the back electrode has the side effect of slightly shifting the resonances towards the IR.

From such two very distinct types of optical cavities, one must design a single one that enhances light absorption following a procedure that simultaneously considers the specific active material absorption curve, the solar spectrum, and possible parasitic absorptions or reflections. An inverse optical cavity design approach is the only viable route provided the resonance structures seen in Figure 1b and 1c do not show any clear indication on how to reach an optical cavity that would exhibit a broadband light trapping. There are four key parameters in such inverse design: the front Ag layer thickness, the active layer thickness, the refractive and thickness of the dielectric layer adjacent to the glass substrate. Other physical

parameters that define the final cell architecture, such as for instance, the thickness of the hole and electron transporting layers, must be kept fixed provided such thickness is to a large extent determined by the electrical rather than the optical performance of the device. Such inverse design should target a cavity configuration that would maximize the short circuit current (J_{SC}) under an AM1.5G 1-sun illumination. As indicated in the section 2 of Supporting Information, for any given range of the parameters above, using a transfer matrix formulation we computed light to electricity conversion for more than 30,000 different cavity configurations to conclude that the optimal DML architecture would be one constructed with a 19 nm TiO_2 layer, a 5 nm ZnO layer, a 5 nm Ag layer, and a second 5 nm ZnO layer combined with a 107 nm active blend layer (See Figure S2, Supporting Information). Note that the thickness of the front Ag layer is well below the standard thickness for such type of semi-transparent electrodes which is typically around 10 nm or above.

2.2 Light trapping in the DML cavity configuration compared to the conventional one

In the limit of geometrical optics, a weak absorption coefficient α, and $\alpha\ell \ll 1$, the fraction of absorbed light can be obtained using equation (1). However, for an estimate of the absorption enhancement applicable to any value of the $\alpha\ell$ product, one must properly consider the build up of internal intensity by multiple light reflections at both active layer interfaces.[9] As shown in the section 3 of the Supporting Information, when the slab is covered by a mirror at the back interface, equation (1) can be replaced by

$$f_{abs} = \frac{W_{abs}}{W_{abs} + W_m + W_{esc}} \qquad (2)$$

where W_{abs} and W_m, are the light energies per unit time and unit surface being absorbed by the active layer and the back mirror, respectively, while W_{esc} is the light intensity that escapes from the cell structure. Although equation (2), as derived in the section 3 of the Supporting Information, is not applicable to cells where the active layer thickness is on the order of 100

nm, one may use it to compute the limit external quantum efficiency (EQE) for a reference cell where the $\alpha(\lambda)\ell$ product is equal to the one of the organic cell we will consider. As active layer we use a ternary bulk-heterojunction blend, consisting of a polymer donor PTB7-Th, fullerene acceptor $PC_{71}BM$ and nonfullerene acceptor FOIC. All the corresponding chemical structures are shown in **Figure 2**a. The configuration used for such reference device was Air/Glass (n=1.52)/Active layer/Mirror (R = 99%), which is the a one providing an optimal enhancement in the fraction of absorbed light according to the conventional limit modified following the derivation in section 3 of the Supporting Information. The EQE or light to electrical charge conversion for such reference cell, which would correspond to a cell with an optical ergodic geometry, is shown in Figure 2b.

As seen in Figure 2b, the predicted EQE for the DML cell configuration is enhanced above the conventional limit of the reference cell for almost the entire absorption range of the photoactive material. Moreover, the inverse design leads to a DML configuration that prioritizes photon absorption in the 700–850 nm range where the number of sun photons is the largest. It is worth noting that using the simple DML 1-dimensionl optical cavity, the conventional light trapping limit can be surpassed for an ample bandwidth larger than 450 nm. Such optimal design of the DML leads to an EQE enhancement averaging above 7 % for most of the absorption band of the active layer and by more than 20% in NIR as seen in Figure 2b. Surpassing the conventional limit is the result of a DML based structure, which, for a large bandwidth, reproduces an almost wavelength independent light trapping, characteristic of a rough surface, with the added advantage of a constructive field superposition. Indeed, for a 5 nm front Ag layer and a TiO_2 thickness close to 19 nm, there is an almost constant relatively high capacity for energy storage as can be seen in Figure 2c.

2.3 DML implementation

The optical role of the DML must not undermine the capacity of the thin metal layer to collect one type of electrical charge, typically electrons in the organic cell configuration we consider. From the results of the inverse design, it is clear that a larger refractive index for the dielectric layer is more effective in breaking the narrow bandwidth of the metal cavity resonances. This must concur with a very homogenous surface for such dielectric layer to achieve a front Ag layer as close as possible to 5 nm. We have found that a high index TiO_2 layer underneath a 5 nm ZnO layer to flatten the roughness and increase the wettability of the TiO_2 surface are the optimal combination for the dielectric part of the DML structure.[37–39] As is well known, physical vapor deposited small quantities of Ag metal tend to cluster into separated island-like grains with Volmer–Weber growth mode, leading to the formation of layers with poor optical and electrical properties.[40,41] To circumvent this tendency, one effective way is to pre-deposit a very thin metal seed layer (～1 nm) such as Au beneath the thin Ag layer,[42,43] but the increased fabrication complexity and cost would not be suitable for large-scale solar cell production. Herein, we use a well-controlled oxygen doping technique to facilitate the uniform and continuous growth of ultrathin Ag films directly on dielectric layers by sputtering an Ag target in a mixture of Ar/O_2 with various flux ratios. Fabrication details can be found in Experimental section.

For a standard ≧10 nm thick Ag layer, that most of the semi-transparent metallic electrodes are made of, a small concentration of O_2 (flux ratio Ar/O_2 = 20:1) is enough for the Ag metal to grow into a homogeneous films without pinholes, as shown in the scanning electron microscope (SEM) image from **Figure 3**a. However, under this condition, it is a great challenge to obtain a high quality thin Ag layer below such thickness. Indeed, for a 7 nm Ag layer grown on such conditions, an island-like discontinuous film, shown in Figure 3b, was observed. By adjusting the Ar/O_2 ratio to 20:3 a pinhole-free and very smooth 7 nm Ag oxide

layer (see Figure 3c and atomic force microscopy images in Figure S5, Supporting Information), with a conductivity similar to the one from a 135 nm thick commercial ITO was obtained. A further reduction of the thickness of the Ag layer, even when further increasing the O_2 concentration, led to a dramatic degradation of the optical as well as electrical properties as shown in Figures 3d and 3e, and Figure S6 (Supporting Information). It is worth noting that even though the Ag in the 7 nm thick film is partially oxidized its optical constants are very similar to those from Palik as confirmed by the DML light transmission measurements seen in Figure 3f. With such constraints on the Ag layer thickness we repeated the inverse design computation targeting again a maximum short circuit current, which yielded the following cell architecture: MgF_2 (110 nm)/glass (refractive index: 1.52)/TiO_2 (25 nm)/ZnO (5 nm)/Ag (7 nm)/ITO (5 nm)/ZnO-SG (10 nm)/PTB7-Th:FOIC:$PC_{71}BM$ (1:0.75:0.75) blend (110 nm)/MoO_3 (5 nm)/Ag (100 nm). The predicted EQE corresponding to this cell architecture can be seen in Figure 2b.

2.4 DML and standard ITO organic cells implementation

With the aim of implementing cells with organic materials exhibiting a bandgap approaching the optimal 1.34 eV gap according to the Shockley-Queisser theory, the organic cells we fabricated are based on the FOIC nonfullerene acceptor that exhibits a band gap close to 1.32 eV. On the other hand, to broaden the absorption band into the blue part of the spectrum, FOIC was mixed with $PC_{71}BM$ at different ratios. Besides that, nonfullerene/$PC_{71}BM$ co-acceptor improves device open circuit voltage (V_{OC}) and fill factor (FF) due to relatively higher LUMO energy level and higher electron mobility in $PC_{71}BM$ as compared to nonfullerene counterparts[38,44]. To determine the optimal acceptor ratio, we carried out several inverse optical design numerical simulations and concluded that a 1:1 weight ratio in the FOIC: $PC_{71}BM$ acceptor blend would exhibit the largest photocurrent when such acceptor blend is mixed in a 1.5:1 weight ratio with PTB7-Th polymer as the electron donor in the bulk

hetero-junction. As can be seen in **Figure 4**a, the optimal 1:1 acceptor ratio is applicable to both the ITO and DML configurations. For the DML architecture, the maximum J_{sc} was numerically determined to be slightly above 25 mA/cm^2, which is approximately 2 mA/cm^2 higher than that of the optimal ITO cell. We fabricated several ITO cells using ternary blends with different FOIC:$PC_{71}BM$ ratios under their optimal conditions (see Table S1 and Figure S7, Supporting Information), and the measured device EQE spectra (Figure S8, Supporting Information) are well matched with the optical simulations, confirming the accuracy of the blend optical constants we measured (See Figure S9, Supporting Information) and that we used in the inverse design.

The averaged PCE increases from 11.0% (standard nonfullerene ITO cell) to 12.2% (1:1 FOIC:$PC_{71}BM$ ITO cell) and further to 13.3% when the DML configuration is implemented. The best-performing *J*-V curves for the three types of cells are shown in Figure 4b. The PCE enhancement here mainly originates from the increase in J_{sc} that the average value jumps by over 2.5 mA/cm^2 from 22.9 mA/cm^2 to 25.6 mA/cm^2 as indicated in Table 1. In addition, when we fabricated smaller size (device area = 0.035 cm^2) DML solar cells, the best efficiency reached 14.16 % due to the improved device *FF*. At the same time the experimental EQE measurements, shown in Figure 4c, confirm the almost wavelength independent EQE predicted by the DML cell inverse optical design, shown in Figure 2b. For such configuration, absorption is enhanced in both the blue and near-infrared regions, confirming an ultra-broadband light absorption above the conventional limit for a wavelengths ranging from 450 to 900 nm. Below ~450 nm the performance of the DML cells is worse than the corresponding ITO reference cell. This can be linked to the Ag plasma frequency which is close to 3.9 eV (318 nm). Above such photon energy, the real part of the dielectric constant becomes positive and the real part of the index becomes very large (See Figure 1S0a, Supporting Information). Essentially, below the plasma frequency but also in its

surroundings the good metal behavior of the Ag layer is lost. Note that as the thickness of such layer increases the EQE of the corresponding cells progressively decreases in the 350-450 wavelength range as seen in Figure S10b of the Supporting Information.

To demonstrate the reliability of such DML approach, we fabricated more than 60 individual devices in different batches under the optimal conditions and a narrow PCE distribution is shown in Figure 4d, indicating very good reproducibility. In addition, DML solar cells exhibited a good stability. After more than 40 days in the dark and ambient conditions encapsulated DML based solar cells showed no signs of degradation as can be seen in Figure S11 in the Supporting Information.

3. Conclusions

A new configuration for an ultra-broadband light trapping is demonstrated by implementing a computationally optimized inverse design. The sub-wavelength structures we have designed and fabricated perform better than optically ergodic ones, which would be obtained from a random texturing of the light entering cell interface. For the most part of the absorption band of the material used in the active layer of the solar cell, the enhancement provided by the DML cavity surpasses by an average of 7% the enhancement that would result from applying the surface randomization that would lead to the conventional limit for light trapping. The inverse deign procedure we implemented leads to a broadband absorption spectrum combined with a high average absorption avoiding resonant peaks that would saturate at 100% absorption, in full compliance with the requirements of a good light trapping design as noted in *Ref*. 10.

As opposed to other light trapping configurations which are meant to be useful when $\alpha\ell \ll 1$, we demonstrate theoretically and experimentally that the DML cavity can be applied when

$\alpha\ell \sim 1$. The large absorption enhancement observed relative to the ergodic geometry, even when the $\alpha\ell$ product is large, proves a universal high capacity for light trapping of the DML configuration when properly designed. Such universal character can be partially confirmed by applying the DML configuration to a different active layer. When FOIC was replaced by IEICO-4F NFA[45], we measured a similar 9% PCE enhancement as can be seen in Figure S12 (Supporting Information). From a practical point of view, the DML is a simple 1-dimensional nanostructured electrode which may not contain Indium and only a small quantity of Ag, most likely leading to a significant cost reduction in an eventual large-scale fabrication of thin film solar modules. In addition, the applicability of such DML cavity configuration is quite general and may be able to perform successfully in other light absorption deficient devices such as high bandgap semiconductor photoanodes in artificial photosynthesis systems meant to carry out the complicated water half oxidation reaction.

4. Experimental Section

Materials and preparation. Polymer PTB7-Th and $PC_{71}BM$ (purity > 99%) were purchased from 1-material and American Dye Source, respectively. FOIC was synthesized by the Zhan group (Peking University). All the materials were used as received without further purification. 2-inch ZnO, TiO_2, Ag and ITO targets were purchased from Kurt J. Lesker Company. Patterned ITO glass substrates (~13 Ω/sq) were purchased from Lumtec. The ternary blend solutions of PCE10:FOIC:$PC_{71}BM$ with various FOIC contents at a total concentration of 25 mg/mL (donor/acceptor = 1:1.5 wt/wt is fixed) were prepared in chlorobenzene (CB) and stirred at 50 ºC overnight in a N_2-filled glovebox. 1, 6-diiodohexane (DIH, 1% Vol) additive was added into the blend mixtures one hour prior to spin-coating. Details on the preparation of 0.15 M sol-gel ZnO precursor can be found elsewhere.[46]

DML fabrication. DML electrodes were sputtered on pre-cleaned Eagle XG glass (Coresix Precision Glass, Inc.) substrates following our previous recipe.[36] The TiO_2, ZnO and ITO films were deposited in a pure Ar atmosphere, while the thin Ag layer was deposited in a mixture of Ar/O_2 (flux ratio 20:3 for 7 nm and 20:1 for above 8 nm, respectively). The ITO thin film was deposited using a DC power of 60 W and a working pressure of 2 mTorr, with deposition rate of 0.65 Å/s. TiO_2 (25 nm)/ZnO (5 nm)/Ag (7 nm)/ITO (5 nm) are sequentially deposited at room temperature without breaking the vacuum chamber. After that, the samples were taken outside for a 10 min thermal annealing at 200 ºC in air. The sheet resistance for the DML electrodes is around 15 Ω/sq.

Solar cell fabrication. ZnO-SG solution was firstly spin coated on the pre-cleaned ITO or as-prepared DML substrates at 5000 rpm for 30 seconds and annealed at 200°C in air (Relative Humidity < 40%) for 20 min to form a ~10 nm electron buffer layer. Then the ZnO coated samples were then transferred into a N_2-filled glove box for spin-casting photoactive layer with the controlled thickness. The resulting blend films were then left in vacuum chamber (kurt J lesker) for one hour to dry under pressure less than 5×10^{-6} mbar. Finally, a 5 nm thick MoO_3 layer (0.4-0.6 Å/s) followed by a 100 nm thick Ag layer (1-1.5 Å/s) were deposited on the active layer through a shadow mask by thermal evaporation (< 5×10^{-6} mbar). The device area, defined by the overlap between transparent electrodes and thick Ag electrodes, was 0.08 cm^2. For DML cells, an additional 110 nm MgF_2 antireflection coating layer was thermally evaporated on the front side of substrates at a rate of 0.5-1 Å/s. All the devices were sealed with glass and UV curable epoxy (DELO KATIOBND LP655) in N_2-filled glovebox before testing in air.

Optical simulations and Characterization. The simulated electromagnetic energy storing capacity, optical transmissions and EQEs were obtained using a home-made computer code

based on the transfer matrix method. The required optical constants (refractive index and extinction coefficient) of all the materials in the device structures were obtained either from modeling the experimental transmission of several thin films with various thicknesses, or from the literature unless stated otherwise. The *J*–V curves of all devices were measured with a Keithley 2420 source meter under a 1 sun, AM 1.5G spectrum from a solar simulator (ABET Sol3A, 1000 W m^{-2}). The illumination intensity of the light source (Xenon lamp, 300W, USHIO) was calibrated using a Hamamatsu silicon photodiode (with KG-5 filter, area = 0.1296 cm^2) certificated by ISE Fraunhofer. Spectrally resolved EQEs were measured using a bench top PV Measurements Inc QEX10 set-up at 130 HZ. The spectral response of the calibrated silicon cell was used as a reference. Optical transmission measurements were performed using a Cary 5000 UV–Vis–NIR spectrophotometer. The sheet resistance of TRTC substrates was determined by a four-point method with cascade Microtech 44/7 S 2749 probe station connected to a Keithley 2001 multimeter. The morphological characteristics of thin-Ag and ternary blend films were studied by field emission scanning electron microscopy (FEG-SEM, FEI Inspect F-EBL) and atomic force microscopy (Veeco, tapping mode).

Supporting Information

Supporting Information is available from the Wiley Online Library or from the author.

Acknowledgements

The authors (Q. L., J. T., M. K., G. M.-D., L.C. and J. M.) acknowledge the financial support from the Spanish Ministry of Economy and Competitiveness (MINECO) through the “Severo Ochoa” program for Centres of Excellence in R&D (SEV-2015-0522), from Fundació Privada Cellex, and from Generalitat de Catalunya through the CERCA program. (Q. L., J. T., M. K., G. M.-D., L.C. and J. M.) also acknowledge financial support from MINECO through

project MAT2017-89522-R and OrgEnergyExcellence Network CTQ2016-81911-REDT. X.Z. thanks the NSFC (No. 21734001). J.M. acknowledges very useful discussions with Luis Pazos-Outón, Joaquim Puigdollers, and Gregory Kozyreff.

Received: ((will be filled in by the editorial staff))
Revised: ((will be filled in by the editorial staff))
Published online: ((will be filled in by the editorial staff))

References

[1] E. Yablonovitch, *J. Opt. Soc. Am.* **1982**, *72*, 27510

[2] T. Tiedje, E. Yablonovitch, G. D. Cody, B. G. Brooks, *IEEE Trans. Electron Devices* **1984**, *31*, 711

[3] E. A. Schiff, *J. Appl. Phys*. **2011**, *110*, 104501.

[4] J. N. Munday, D. M. Callahan, H. A. Atwater, *Appl. Phys. Lett*. **2012**, *100*, 121121.

[5] Z. Yu, A. Raman, S. Fan, *Proc. Natl. Acad. Sci*. **2010**, *107*, 17491–17496.

[6] K. X. Wang, Z. Yu, V. Liu, A. Raman, Y. Cui, S. Fan, *Energy Environ. Sci.* **2014**, *7*, 2725–2738.

[7] M. A. Green, *Prog. Photovoltaics Res. Appl.* **2011**, *19*, 473–477.

[8] J. Grandidier, D. M. Callahan, J. N. Munday, H. A. Atwater, *Adv. Mater.* **2011**, *23*, 1272–1276.

[9] D. M. Callahan, J. N. Munday, H. A. Atwater, *Nano Lett.* **2012**, *12*, 214–218.

[10] J. Wallentin, N. Anttu, D. Asoli, M. Huffman, I. Åberg, M. H. Magnusson, G. Siefer, P. Fuss-Kailuweit, F. Dimroth, B. Witzigmann, H. Q. Xu, L. Samuelson, K. Deppert, M. T. Borgström, *Science.* **2013**, *339*, 1057–1060.

[11] M. L. Brongersma, Y. Cui, S. Fan, *Nat. Mater.* **2014**, *13*, 451–460.

[12] L. M. Pazos-Outón, T. P. Xiao, E. Yablonovitch, *J. Phys. Chem. Lett.* **2018**, *9*, 1703–1711.

[13] V. Ganapati, O. D. Miller, E. Yablonovitch, *IEEE J. Photovoltaics* **2014**, *4*, 175–182.

[14] T. Li, S. Dai, Z. Ke, L. Yang, J. Wang, C. Yan, W. Ma, X. Zhan, *Adv. Mater.* **2018**, *30*, 1705969.

[15] W. Shockley, H. J. Queisser, *J. Appl. Phys.* **1961**, *32*, 510–519.

[16] W. Zhao, D. Qian, S. Zhang, S. Li, O. Inganäs, F. Gao, J. Hou, *Adv. Mater.* **2016**, *28*, 4734–4739.

[17] J. Liu, S. Chen, D. Qian, B. Gautam, G. Yang, J. Zhao, J. Bergqvist, F. Zhang, W. Ma, H. Ade, O. Inganäs, K. Gundogdu, F. Gao, H. Yan, *Nat. Energy* **2016**, *1*, 16089.

[18] J. Zhang, Y. Li, J. Huang, H. Hu, G. Zhang, T. Ma, P. C. Y. Chow, H. Ade, D. Pan, H. Yan, *J. Am. Chem. Soc.* **2017**, *139*, 16092–16095.

[19] X. Liu, X. Du, J. Wang, C. Duan, X. Tang, T. Heumueller, G. Liu, Y. Li, Z. Wang, J. Wang, F. Liu, N. Li, C. J. Brabec, F. Huang, Y. Cao, *Adv. Energy Mater.* **2018**, *8*, 1801699.

[20] X. K. Chen, J. L. Brédas, *Adv. Energy Mater.***2018***, 8,* 1702227.

[21] X. Xu, Z. Li, W. Zhang, X. Meng, X. Zou, D. Di Carlo Rasi, W. Ma, A. Yartsev, M. R. Andersson, R. A. J. Janssen, E. Wang, *Adv. Energy Mater.* **2018**, *8*, 1700908.

[22] D. Yang, Y. Wang, T. Sano, F. Gao, H. Sasabe, J. Kido, *J. Mater. Chem. A* **2018**, *6*, 13918–13924.

[23] D. Qian, Z. Zheng, H. Yao, W. Tress, T. R. Hopper, S. Chen, S. Li, J. Liu, S. Chen, J. Zhang, X. K. Liu, B. Gao, L. Ouyang, Y. Jin, G. Pozina, I. A. Buyanova, W. M. Chen, O. Inganäs, V. Coropceanu, J. L. Bredas, H. Yan, J. Hou, F. Zhang, A. A. Bakulin, F. Gao, *Nat. Mater.* **2018**, *17*, 703–709.

[24] Y. Lin, J. Wang, Z. G. Zhang, H. Bai, Y. Li, D. Zhu, X. Zhan, *Adv. Mater.* **2015**, *27*, 1170–1174.

[25] S. Dai, F. Zhao, Q. Zhang, T. K. Lau, T. Li, K. Liu, Q. Ling, C. Wang, X. Lu, W. You, X. Zhan, *J. Am. Chem. Soc.* **2017**, *139*, 1336–1343.

[26] S. Dai, T. Li, W. Wang, Y. Xiao, T. K. Lau, Z. Li, K. Liu, X. Lu, X. Zhan, *Adv. Mater.* **2018**, *30*, 1706571.

[27] W. Jiang, R. Yu, Z. Liu, R. Peng, D. Mi, L. Hong, Q. Wei, J. Hou, Y. Kuang, Z. Ge, *Adv. Mater*. **2018**, *30*, 1703005.

[28] J. Hou, O. Inganas, R. H. Friend, F. Gao, *Nat. Mater.* **2018**, *17*, 119–128.

[29] C. Yan, S. Barlow, Z. Wang, H. Yan, A. K. Y. Jen, S. R. Marder, X. Zhan, *Nat. Rev. Mater.* **2018,** *3*, 18003.

[30] P. Cheng, G. Li, X. Zhan, Y. Yang, *Nat. Photonics* **2018**, *12*, 131–142.

[31] G. Zhang, J. Zhao, P. C. Y. Chow, K. Jiang, J. Zhang, Z. Zhu, J. Zhang, F. Huang, H. Yan, *Chem. Rev.* **2018**, *118*, 3447–3507.

[32] C. Zhang, D. Zhao, D. Gu, H. Kim, T. Ling, Y. K. R. Wu, L. J. Guo, *Adv. Mater.* **2014**, *26*, 5696–5701.

[33] J. Huang, C. Z. Li, C. C. Chueh, S. Q. Liu, J. S. Yu, A. K. Y. Jen, *Adv. Energy Mater.* **2015**, *5*, 1500406.

[34] D. S. Ghosh, Q. Liu, P. Mantilla-Perez, T. L. Chen, V. Mkhitaryan, M. Huang, S. Garner, J. Martorell, V. Pruneri, *Adv. Funct. Mater.* **2015**, *25*, 7309–7316.

[35] A. T. Barrows, R. Masters, A. J. Pearson, C. Rodenburg, D. G. Lidzey, *Sol. Energy Mater. Sol. Cells* **2016**, ***144***, 600–607.

[36] Q. Liu, P. Romero-Gomez, P. Mantilla-Perez, S. Colodrero, J. Toudert, J. Martorell, *Adv. Energy Mater.* **2017**, *7*, 1700356.

[37] S. Schubert, M. Hermenau, J. Meiss, L. M??ller-Meskamp, K. Leo, *Adv. Funct. Mater.* **2012**, *22*, 4993–4999.

[38] Q. Liu, J. Toudert, L. Ciammaruchi, G. Martínez-Denegri, J. Martorell, *J. Mater. Chem. A* **2017**, *5*, 25476–25484.

[39] G. Zhao, W. Shen, E. Jeong, S. G. Lee, S. M. Yu, T. S. Bae, G. H. Lee, S. Z. Han, J. Tang, E. A. Choi, J. Yun, *ACS Appl. Mater. Interfaces* **2018**, *10*, 27510–27520.

[40] J. Yun, W. Wang, T. S. Bae, Y. H. Park, Y. C. Kang, D. H. Kim, S. Lee, G. H. Lee, M. Song, J. W. Kang, *ACS Appl. Mater. Interfaces* **2013**, *5*, 9933–9941.

[41] J. Yun, *Adv. Funct. Mater.* **2017**, *27*, 1606641.

[42] S. Schubert, J. Meiss, L. Müller-Meskamp, K. Leo, *Adv. Energy Mater.* **2013**, *3*, 438–443.

[43] H. R. Colenso, E. Z. Rafealov, M. Maddah, N. O. V. Plank, W. T. Chen, G. I. N. Waterhouse, J. Hao, G. J. Gouws, C. P. Moore, *Thin Solid Films* **2018**, *656*, 68–74.

[44] H. Lu, J. Zhang, J. Chen, Q. Liu, X. Gong, S. Feng, X. Xu, W. Ma, Z. Bo, *Adv. Mater.* **2016**. *28*, 9559–9566.

[45] H. F. Yao, Y. C. R. N. Yu, B. W. Gao, H. Zhang, J. H. Hou, Angew. *Chem., Int. Ed*., **2017**, *56*, 3045.

[46] Q. Liu, P. Mantilla-Perez, M. Montes Bajo, P. Romero-Gomez, J. Martorell, *ACS Appl. Mater. Interfaces* **2016**, *8*, 28750–28756.

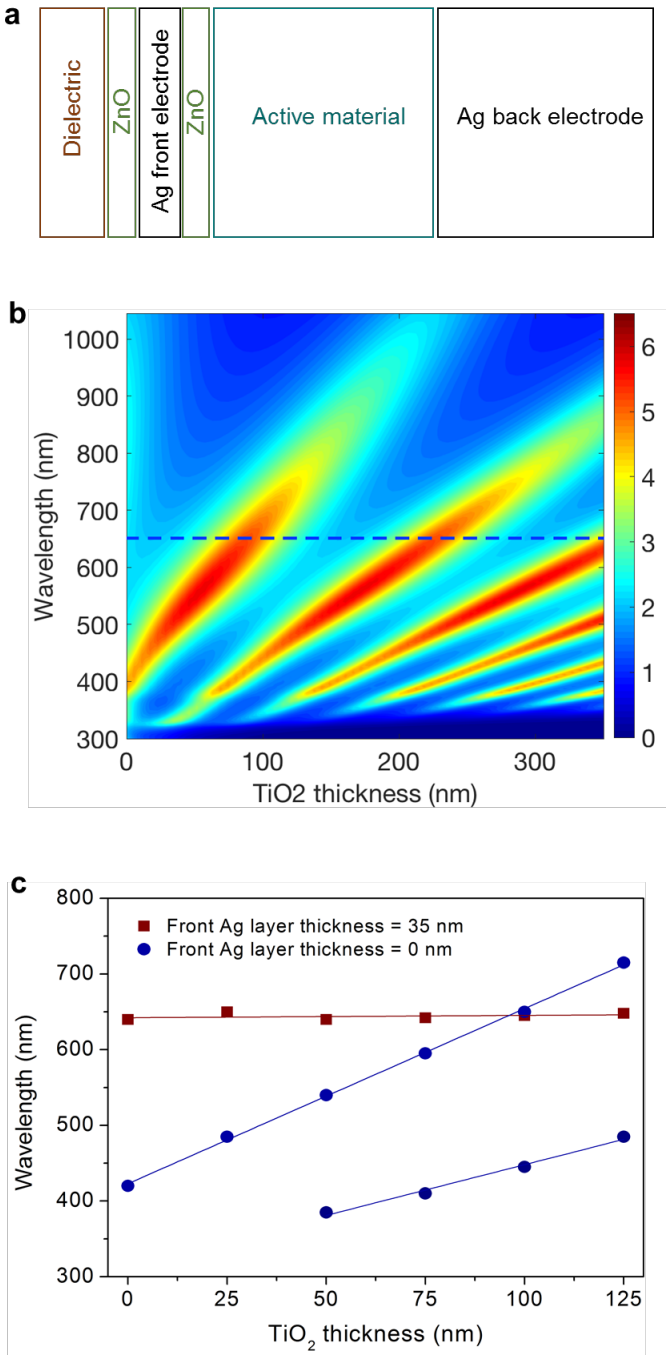

Figure 1. Optical cavity inverse design. (a) Schematic representation of the DML optical cavity. (b) Electromagnetic energy storage resonance structure (vertical axis) for the DML cavity when the thickness of the first metal layer is reduced to 0 as a function of the wavelength (y-axis) and the thickness of the dielectric layer (x-axis). The dashed line indicates the position of the DML cavity resonance when the thickness of the first metal layer is large. (c) Measured transmission resonances (peaks) for the DML cavity in the two limiting cases. The cavity structure is glass/TiO_2 (0–125 nm)/ZnO (5 nm)/Ag (0 and 35 nm)/ZnO (5 nm)/MoO_3 (115 nm)/Ag (25 nm). The solid lines presents the best linear fittings of the experimental data.

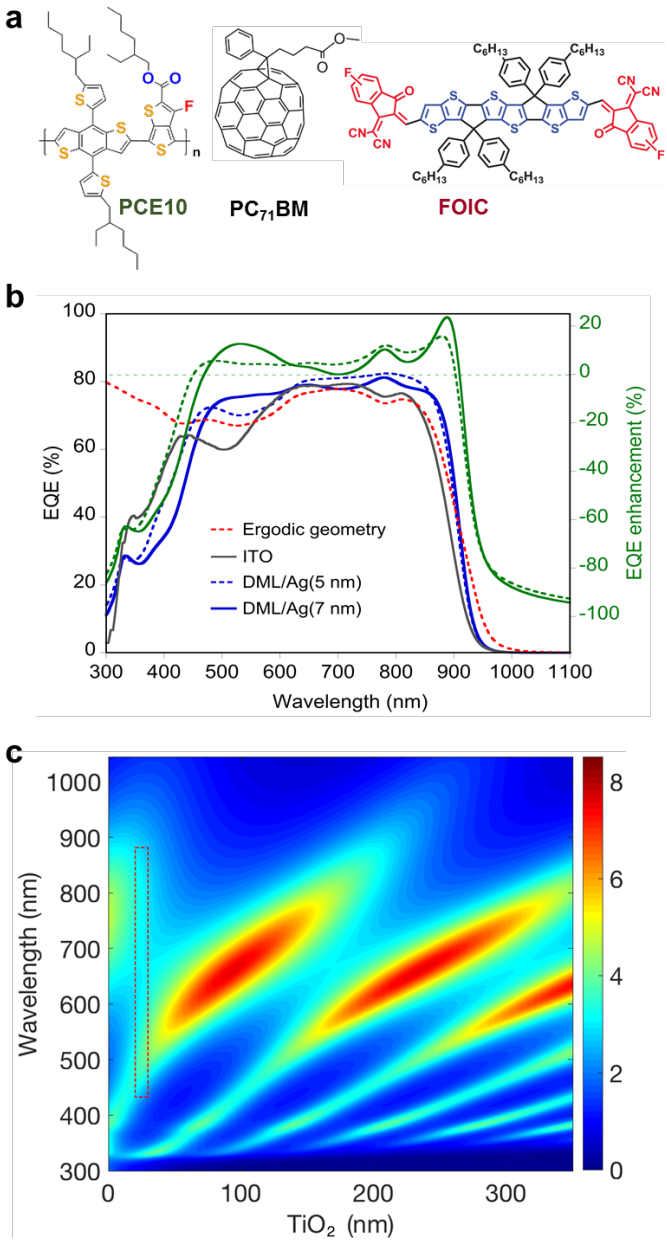

Figure 2. Light trapping & absorption in the DML configuration. . (a) Chemical structures of used active material consisting of PTB7-Th polymer, $PC_{71}BM$ fullerene acceptor and FOIC nonfullerene acceptor. (b) Left axis: Computed EQEs when the $\alpha\ell$ product is equivalent to the one from a 107 nm thick active layer of the used organic blend in: a standard ITO cell configuration (solid grey line), the DML cell configuration with an Ag front electrode of 7 nm (solid blue line) and 5 nm Ag (dashed blue line), an optical ergodic geometry configuration with a 99% wavelength independent reflectivity back mirror (dashed red line). Right axis: EQE percentage enhancement for DML cells with a 7 nm (solid green line) and a 5 nm (dashed green line) Ag front electrode relative to the optical ergodic geometry configuration. The optical constants used for the active layer are from the optimal ternary blend of PTB7-Th:FOIC:$PC_{71}BM$ (1:0.75:0.75). (c) Energy storing capacity (vertical axis) of the DML cavity configuration as a function of the wavelength and dielectric layer thickness. A dashed rectangle indicates the broadband energy storage region.

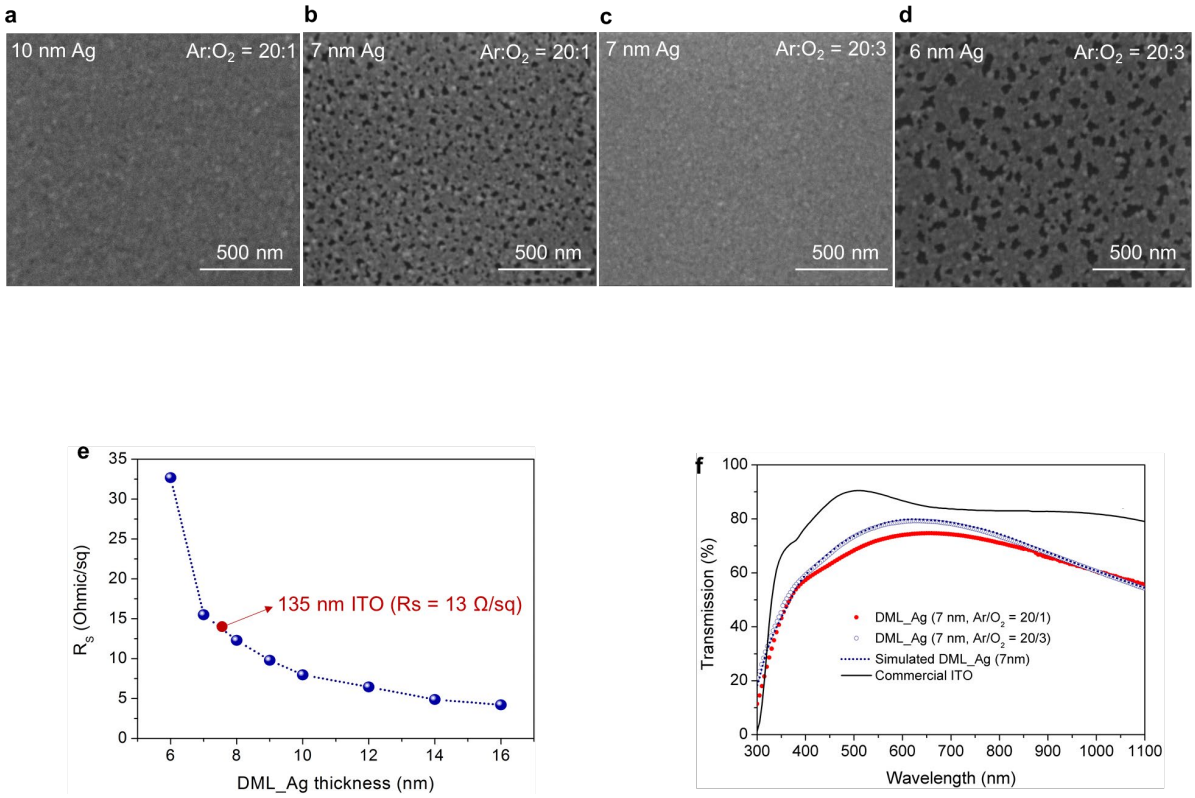

Figure 3. Morphology and electrical/optical properties of the thin-Ag layer. SEM images of glass/TiO_2 (25 nm)/ZnO (5 nm)/thin Ag samples. (a) 10 nm Ag layer was sputtered from a mixture of Ar/O_2 at flux ratio of 20:1; (b) and (c) are 7 nm Ag layers sputtered from a mixture of Ar/O_2 at flux ratio of 20:1 and 20:3, respectively. (d) 6 nm Ag layer deposited from a Ar/O_2 = 20:3 mixture. (e) Sheet resistance of glass/TiO_2 (25 nm)/ZnO (5 nm)/Ag/ITO (5 nm) electrodes as function of the thin-Ag thickness. The red point indicates the sheet resistance of typical commercial ITO substrates. (f) The transmission spectra of fused silica substrate/TiO_2 (25 nm)/ZnO (5 nm)/Ag (7 nm)/ITO (5 nm) electrodes and the commercial ITO as the reference is also indicated.

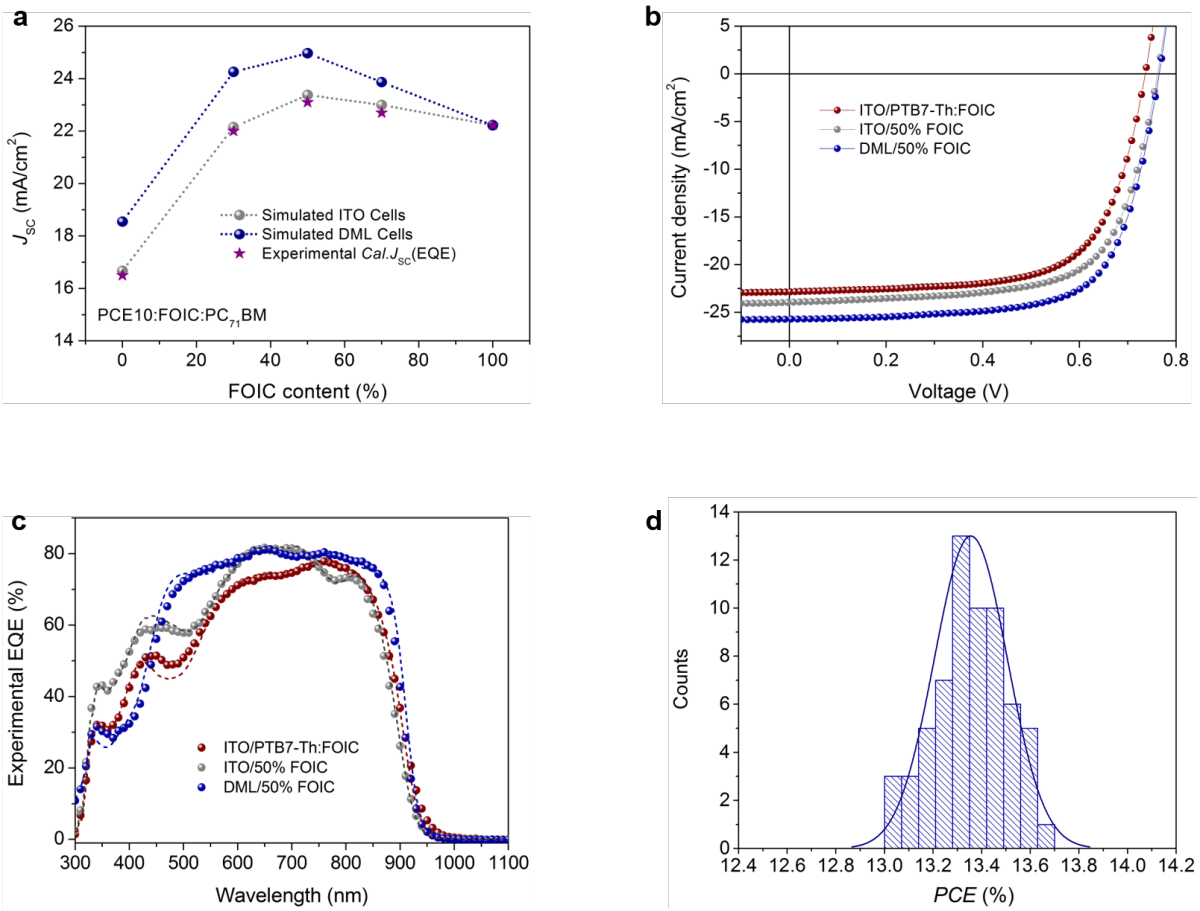

Figure 4. Experimental implementation of DML solar cells. (a) Numerically computed J_{SC} as function of FOIC content in the ternary blends for ITO and TRTC configurations, and the integrated J_{SC} (star point) from experimental EQEs of ITO cells are indicated. Here, the internal quantum efficiency (IQE) for simulations are estimated to 0.88. (b) *J*-V curves of the best-performing ITO nonfullerene cell (red dots), 50% FOIC ITO cell (gray dots) and DML 50% FOIC cell (blue dots) measured under AM 1.5G illumination at 100 mW cm^{-2} (c) Experimentally measured (dots) and simulated (dashed lines) EQEs for the corresponding cells. (d) PCE distribution for 50% FOIC DML devices based on 63 devices.

Table 1. Photovoltaic parameters for ITO and DML solar cells under AM 1.5G solar illumination at 1000 W m^{-2}.

Device structure	Active layer	J_{sc} (J_{EQE})[a] [mA cm^{-2}]	V_{oc} [V]	*FF* [%]	*PCE*[b] [%]
ITO	PTB7-Th: FOIC (Standard)	22.94 ± 0.27 (22.2)	0.734 ± 0.002	65.33 ± 1.0	11.01 ± 0.12 (11.26)
ITO	PTB7-Th:FOIC:$PC_{71}BM$ (50% FOIC)	23.89 ± 0.19 (23.1)	0.758 ± 0.002	66.96 ± 1.1	12.20 ± 0.25 (12.57)
DML	PTB7-Th:FOIC:$PC_{71}BM$ (50% FOIC)	25.68 ± 0.16 (24.7)	0.764 ± 0.002	67.9 ± 0.9	13.35 ± 0.19 (13.64)
		25.58 ± 0.13 (24.7)	0.765 ± 0.002	71.6 ± 0.4	13.87 ± 0.27 (14.16)[c]

[a] Calculated from experimental EQE spectra. [b] The average values and standard deviations are obtained from over 20 devices and the best PCE values are shown in the parentheses. DML here presents MgF_2 (110nm)/glass substrate/TiO_2 (25 nm)/ZnO (5nm)/Ag (7 nm)/ITO (5 nm). [c] Device area = 0.035 cm^2.

The table of contents.

A 1-dimensional ultra-broadband (> 450 nm) optical cavity is designed following an inverse electromagnetic computational approach to optimally trap light in a thin film absorber layer. When this novel cavity concept is applied to a low bandgap organic solar cell, we demonstrate a broadband absorption enhancement beyond to the conventional limit resulting from light trapping in an ergodic optical geometry.

Keywords: Light trapping, optical cavity, ternary blend, low-bandgap nonfullerene acceptor thin-film solar cell

Dr. Q. Liu[1], Dr. J. Toudert[1], T. Li[2], M. Kramarenko[1], G. Martínez-Denegri[1], Dr. L. Ciammaruchi[1], Prof. X. Zhan[2]* and Prof. J. Martorell[1,3]*

Title: Inverse optical cavity design for ultrabroadband light absorption beyond the conventional limit in low-bandgap nonfullerene acceptor based solar cells